

Terahertz Coherent Control of Optically Dark Paraexcitons in Cu₂O

S. Leinß,¹ T. Kampfrath,² K. v. Volkmann,² M. Wolf,² J. T. Steiner,³ M. Kira,³ S. W. Koch,³ A. Leitenstorfer,¹ and R. Huber¹

¹*Fachbereich Physik, Universität Konstanz, Fach M 696, 78457 Konstanz, Germany*

²*Fachbereich Physik, Freie Universität Berlin, Arnimallee 14, 14195 Berlin, Germany*

³*Fachbereich Physik, Universität Marburg, Renthof 5, 35032 Marburg, Germany*

(Received 5 September 2008; published 10 December 2008)

Intense multiterahertz fields of order megavolts per centimeter are used to coherently promote optically dark and dense paraexcitons in Cu₂O from the *1s* into the *2p* state. The nonlinear field response of the intraexcitonic degrees of freedom is directly monitored in the time domain via ultrabroadband electro-optic sampling. The experimental results are analyzed with a microscopic many-body theory, identifying up to two internal Rabi cycles. The effects of population inversion and ponderomotive contributions are disentangled.

DOI: 10.1103/PhysRevLett.101.246401

PACS numbers: 71.35.Lk, 78.47.-p, 42.65.-k

Nonlinear optical control of dilute atomic gases has produced a fascinating success story, culminating in efficient techniques of laser cooling and the first demonstration of Bose-Einstein condensation (BEC) [1]. Excitons—Coulomb-bound pairs of one electron and one hole (*e-h* pairs)—have been discussed as another potential candidate for BEC [2,3]. Recent reports of quantum degeneracy in the related system of exciton polaritons have refueled these hopes [4]. Yet it is a fundamental challenge to control excitons that are relevant for BEC by conventional optical techniques because these quasiparticles often exhibit weak if any coupling to visible radiation.

The *1s* excitons of the yellow series in Cu₂O illustrate this dilemma drastically [2,3,5–10]: Strong exchange interaction splits the *1s* ground state (binding energy: 150 meV) by 12 meV into a triply degenerate Γ_5^+ ortho and a lower-lying nondegenerate Γ_2^+ para variety. While interband recombination of ortho excitons is dipole forbidden, para states are optically dark to all multipole orders due to their spin of unity. This fact ensures long lifetimes on the microsecond scale and thus makes *1s* paraexcitons interesting for quasiequilibrium BEC [3,5]. On the other hand, spin conservation also prohibits the direct observation and control of para states via optical interband transitions.

Terahertz (THz) pulses couple directly to the internal excitations of quasiparticles, irrespective of interband matrix elements [5,8,9,11–15]. Studies of intraexcitonic absorption have provided novel insight into the formation dynamics, fine structure, density, and temperature of excitons [5,13]. The recent observation of the inverse quantum process of stimulated THz emission from internal *3p-2s* transitions in Cu₂O has raised the hope for future control of dark excitons via coherent THz nonlinearities [8]. First experiments exposing excitons to intense THz and infrared fields have focused on the optical Stark effect and the dynamic Franz-Keldysh effect. These processes modify interband transitions [16–18] and are thus limited to bright excitons.

In this Letter, we explore the nonlinear THz response of optically dark excitons: Intense THz transients are exploited to control the orbital degree of freedom of a dense gas of cold paraexcitons in Cu₂O. Field-sensitive electro-optic sampling of the internal polarization response allows us to trace the quantum dynamics while *1s* excitons are coherently excited into the *2p* state. For the highest pulse energies achieved, the reemitted THz field displays an oscillatory temporal envelope and nonmonotonic dependence on the driving pulse area. These results are direct evidence of a coherent nonlinearity consistent with up to two intraexcitonic Rabi cycles. We simulate the nonlinear THz response with a microscopic theory and discuss the importance of transitions to higher bound and unbound exciton states as well as ponderomotive terms.

Our sample is a naturally grown single crystal of Cu₂O (thickness: 264 μm) kept at a temperature of $T_L = 5$ K. In a first step, we characterize the formation dynamics of *1s* paraexcitons by multi-THz probes of the *1s-2p* transition. The corresponding Lyman lines are expected at photon energies of 116 and 129 meV for ortho and para states, respectively [5]. For this experiment, we employ a low-noise Ti:sapphire amplifier for intense 12-fs pulses centered at a photon energy of 1.55 eV (repetition rate: 0.8 MHz). Part of the output creates unbound *e-h* pairs with a homogeneous density of $n_{e-h} = 2 \times 10^{16} \text{ cm}^{-3}$ via two-photon absorption. A second branch generates multi-THz pulses by optical rectification in GaSe. These transients are transmitted through the sample. Phase-matched electro-optic detection [19] yields the temporal waveform of the probe field for selected delay times t_D between the near-infrared pump and the THz probe. This two-dimensional scheme [12] affords simultaneous access to pump-induced changes of the absorption coefficient and the refractive index as a function of t_D [Fig. 1(a)].

Starting with an almost Drude-like response of the photogenerated unbound *e-h* pairs, at $t_D = 100$ fs, the spectra change dramatically on a few-picosecond scale. The positive slope of the measured differential absorption $\Delta\alpha$ at

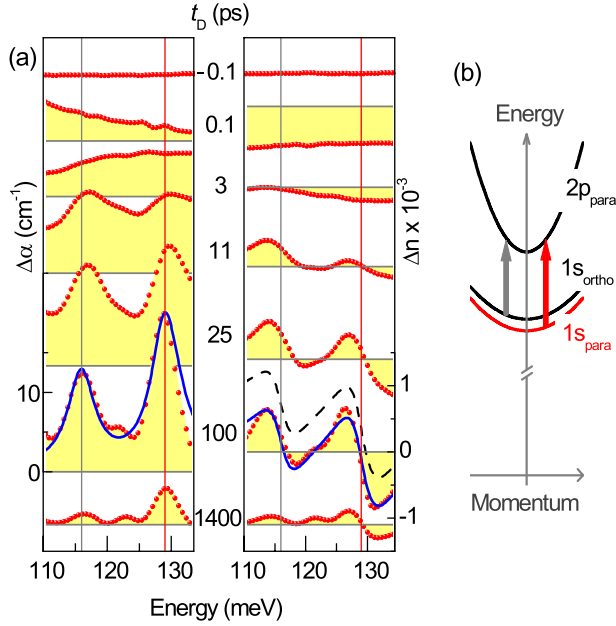


FIG. 1 (color online). (a) Formation and cooling dynamics of $1s$ excitons in Cu_2O probed by multi-THz spectroscopy: Pump-induced changes of absorption $\Delta\alpha$ and refractive index Δn (shaded area with dots) for various delay times t_D after two-photon absorption of 12-fs pulses centered at 1.55 eV. Vertical lines: $1s$ - $2p$ resonances at vanishing center-of-mass momentum. Solid line: Theoretical result with $n_{1s}^{\text{para}} = 1 \times 10^{16} \text{ cm}^{-3}$, $n_{1s}^{\text{ortho}} = 0.5 \times 10^{16} \text{ cm}^{-3}$, and $T_{1s} = 10 \text{ K}$. Dashed line: Theoretical Δn without ponderomotive contribution. (b) Because of different effective masses of $1s$ and $2p$ excitons, THz transitions (arrows) depend on the center-of-mass momentum.

$t_D = 3 \text{ ps}$ indicates an emerging low-energy gap in the excitation spectrum of an insulating phase of hot excitons. After $t_D = 11 \text{ ps}$, the hallmark $1s$ - $2p$ lines attest to a population of $1s$ para and ortho states [5]. Exciton formation in Cu_2O thus proceeds substantially faster than in III-V semiconductors [13,20] and is directly resolved here. Both intraexcitonic lines narrow and shift to lower frequencies during the first 100 ps, while the ratio of para versus ortho densities increases. Because of different effective masses of $1s$ and $2p$ states [Fig. 1(b)], the temperature T_{1s} of the ensemble is encoded in the THz line shape [5,7,9]. We compare the experimental response for $t_D = 100 \text{ ps}$ to results from our microscopic theory introduced below. With a dipole moment $\mu_{1s-2p} = 3.5 \pm 0.3 \text{ e}\text{\AA}$ obtained from a realistic band structure calculation [21], we find good agreement when we assume densities of $n_{1s}^{\text{para}} = (1 \pm 0.2) \times 10^{16} \text{ cm}^{-3}$ and $n_{1s}^{\text{ortho}} = (0.5 \pm 0.1) \times 10^{16} \text{ cm}^{-3}$ and a temperature of $T_{1s} = 10 \pm 4 \text{ K}$ [Fig. 1(a)]. n_{1s}^{para} is thus approximately 1 order of magnitude below critical values for potential BEC. The rapid cooling close to T_L confirms a highly efficient exciton-phonon coupling [20]. For delay times $t_D > 100 \text{ ps}$, an additional less pronounced absorption maximum, not included in our model, evolves

at an energy of 123 meV. Its potential relation with biexcitonic resonances [22] is currently under investigation.

In the next step, we actively control the internal quantum state of the dark quasiparticles. To this end, we replace the broadband probe with an intense THz transient E_{THz} generated resonantly to the $1s$ - $2p$ para transition (photon energy: 129 meV; width: 4 meV) by optical rectification of 0.2 mJ pulses from a high-power Ti:sapphire amplifier (repetition rate: 1 kHz) [23]. Optimally shaped laser pulses from an acousto-optic modulator and tight focusing of the multi-THz beam to a diffraction limited spot of $35 \mu\text{m}$ (FWHM of the field) allow us to reach peak fields of $E_{\text{THz}}^{\text{peak}} = (0.5 \pm 0.15) \text{ MV/cm}$ [Fig. 2(a)].

Curves (i)–(vi) in Fig. 2(a) represent the response of $1s$ paraexcitons to the incident waveform E_{THz} at six different peak fields $E_{\text{THz}}^{\text{peak}}$. All THz field traces are recorded directly in the time domain by electro-optic detection. At low excitation intensity [curves (i) and (ii)], the reemitted field reaches its maximum towards the end of the driving pulse E_{THz} and then decays with a finite dephasing time of 0.7 ps. Strikingly, for intermediate and high intensities of the driving field [curves (iii)–(vi)], the response is not a linearly increased version of the low-field case. Rather, the reemitted field rises more rapidly, reaches its maximum before the peak of the pump transient, and decreases within the coherence window. Also, the maximum value of the amplitude saturates for increasing excitation density. This intensity-dependent response, in particular the temporal shift of the amplitude maximum from $T = 0.25 \text{ ps}$ [curve (i)] to $T = -0.25 \text{ ps}$ [curve (vi)], shows clearly that the THz field saturates the $1s$ - $2p$ transition inducing a coherent nonlinearity. Most remarkably, curves (v) and (vi) exhibit a structured envelope with a first maximum at $T = -0.25 \text{ ps}$ and a second less pronounced side peak at 0.25 ps (v) and 0.24 ps (vi), respectively. The onset of an oscillatory behavior indicates that the intense THz beam leads to nonlinear dynamics of dark exciton populations well beyond the perturbative regime.

In order to analyze the experimental results, we apply a microscopic description of intraexcitonic light-matter coupling and dynamics [15,24,25]. The THz response follows from Maxwell's wave equation

$$\left[\nabla^2 - \frac{n_0^2}{c^2} \frac{\partial^2}{\partial t^2} \right] A_{\text{THz}} = -\mu_0 (J_{\text{THz}} + J_A) \quad (1)$$

for the vector potential A_{THz} , which is related to the electric field via $E_{\text{THz}} = -\frac{\partial}{\partial t} A_{\text{THz}}$. Here c is the speed of light, n_0 the background refractive index of the medium, and μ_0 the vacuum permittivity. The right-hand side of Eq. (1) consists of two contributions: (i) The THz current $J_{\text{THz}} = \frac{1}{V} \sum_{\lambda, \mathbf{k}} j_{\lambda}(\mathbf{k}) f_{\mathbf{k}}^{\lambda}$, with quantization volume V , depends on the occupation probability $f_{\mathbf{k}}^{\lambda}$ of an electron with momentum \mathbf{k} in band λ and the current-matrix element $j_{\lambda}(\mathbf{k}) = -\frac{|e|}{\hbar} \frac{\partial \varepsilon_{\mathbf{k}}^{\lambda}}{\partial \mathbf{k}} \cdot \mathbf{e}_A$. Here $\varepsilon_{\mathbf{k}}^{\lambda}$ describes the band structure, and \mathbf{e}_A

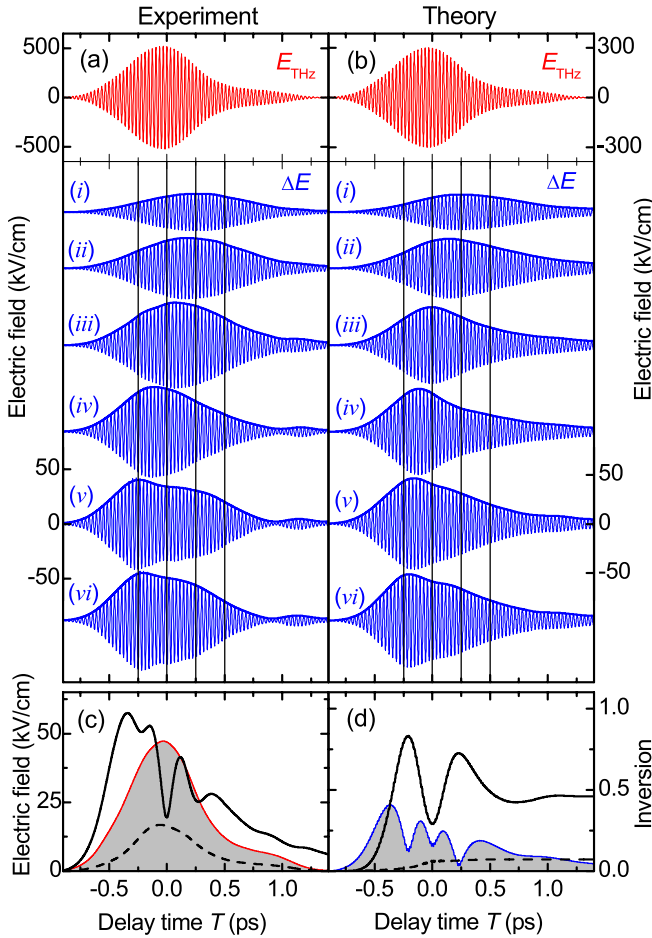


FIG. 2 (color online). Nonlinear THz response of $1s$ paraexcitons ($t_D = 1$ ns): quantitative comparison of (a) experiment and (b) microscopic theory. Upper panels: Real-time profile of the exciting THz pulse E_{THz} . Lower panels: Reemitted THz field ΔE (vertically offset) for six values of the peak driving field, with $E_{\text{THz}}^{\text{peak}} = 0.13, 0.24, 0.45, 0.67, \text{ and } 0.92, 1.0 \times E_0$ for curves (i)–(vi), respectively ($E_0 = 0.5$ MV/cm in experiment and $E_0 = 0.3$ MV/cm in theory). (c) Theoretical transient for the highest intensity. The envelopes of ΔE_A (dashed curve) and ΔE (solid curve) at the spot center are shown together with the scaled excitation pulse (shaded area). (d) Inversion (solid curve) and polarization (shaded area) of the two-level system consisting of $1s$ and $2p$ paraexciton states as well as ionized exciton fraction (dashed curve) at the center of the THz spot.

denotes the polarization direction of the THz field. For the thermalized initial conditions studied here, J_{THz} results from the many-body dynamics of exciton populations [15,25]. (ii) The ponderomotive current $J_A = -\frac{e^2}{\hbar^2 V} \sum_{\mathbf{k}, \lambda} \frac{\partial^2 \epsilon_{\mathbf{k}}^\lambda}{\partial |\mathbf{k}|^2} f_{\mathbf{k}}^\lambda A_{\text{THz}}$ does not directly couple to the many-body dynamics. For the thin samples used in this work, the reemitted field ΔE is proportional to the total induced current $J = J_{\text{THz}} + J_A$.

In the linear susceptibility, the ponderomotive current yields a real-valued Drude-like contribution $\chi_A(\omega) = -\omega_{\text{PL}}^2/\omega^2$ which gives rise to a refractive index change;

the absorption shown in Fig. 1(a) follows entirely from J_{THz} . In the limit of parabolic bands, ω_{PL}^2 is identical to the three-dimensional plasma frequency $ne^2/(\epsilon_0\mu)$, with carrier density n and reduced effective mass μ . The measured refractive index change for $t_D = 100$ ps [shaded area with dots in Fig. 1(a)] is explained only by the full theory (solid line) in contrast to calculations without the ponderomotive contribution (dashed line).

To evaluate the nonlinear response, we solve the current dynamics using the exact temporal and spatial profile of the experimental excitation pulses and a realistic band structure of Cu_2O [21]. The nonparabolicity of the electronic energy dispersion accounts for the anomalously large $1s$ binding energy and for the center-of-mass dependence of exciton energies and matrix elements. All exciton levels with s -, p -, and d -like symmetry including the continuum states are taken into account. We assume that initially all electron-hole pairs exist as $1s$ paraexcitons. Since the density of ortho states is low for large times t_D and their $1s$ - $2p$ transition is nonresonant to the external field, their contribution is negligible. Finally, the Gaussian TEM_{00} spatial distribution of the THz field results in a significant averaging of the THz intensity. The only adjustable parameters are the maximum field E_0 and an intraexcitonic dephasing time. The calculated reemitted fields ΔE [Fig. 2(b)] reproduce all key signatures of Fig. 2(a), including the temporal shift and saturation of the maximum amplitude as well as the structured envelope for the two highest intensities.

In Fig. 2(c), we analyze the theoretical envelope of $\Delta E = \Delta E_{\text{THz}} + \Delta E_A$ for the highest excitation intensity [curve (vi) in Fig. 2(b)] in more detail. Here ΔE_{THz} results from excitonic transitions, and ΔE_A is the ponderomotive term. While ΔE_A [dashed line in Fig. 2(c)] contributes significantly, the main response results from ΔE_{THz} . In particular, the envelope of ΔE_A closely follows the external pulse shape (shaded area) such that the oscillatory features in the total signal must derive exclusively from ΔE_{THz} .

To reveal the origin of these oscillations, we compute the dynamics of exciton populations at the center of the THz spot where the intensity is highest [Fig. 2(d)]. We find that the population inversion (solid line) as well as the absolute value of the polarization (shaded area) of the $1s$ - $2p$ two-level subsystem exhibit approximately two Rabi oscillation cycles. The $1s$ - $2p$ inversion reaches a maximum value of $(80 \pm 5)\%$, while the fraction of ionized excitons (dashed line) remains well below 10%. Strong oscillations of the envelope of the reemitted field are obtained at the spot center [solid line in Fig. 2(c)]. Because of the Gaussian THz field distribution, the total detected signal ΔE averages over various pulse areas and hence displays only residual Rabi oscillations. We note that experiments under more homogeneous spatial excitation conditions will be possible as soon as high-field THz sources with larger pulse energies are available.

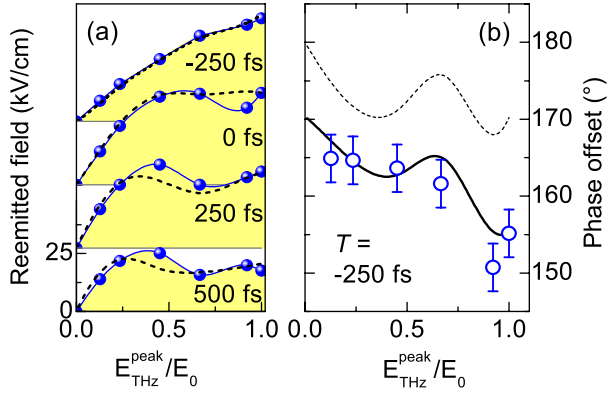


FIG. 3 (color online). (a) Reemitted THz amplitude versus maximum $E_{\text{THz}}^{\text{peak}}$ of the driving field at four delay times T , extracted from Fig. 2; circles and shaded areas: experiment; connecting thin curves: guides to the eye; dashed curves: simulation ($E_0 = 0.5$ MV/cm in experiment and $E_0 = 0.3$ MV/cm in theory). (b) Phase offset between pump-induced and driving fields at a preset time $T = -0.25$ ps obtained from Fig. 2. Experiment (circles) and theory with (solid curve) and without (dashed curve) a ponderomotive part are shown.

In Fig. 3, we investigate the intensity dependence of the THz transients. Cross sections of the field envelopes of Fig. 2 are plotted at four different delay times T [vertical lines in Figs. 2(a) and 2(b)]. Again, we find close agreement between experiment (circles) and theory (dashed lines). For $T = -0.25$ ps [top curve in Fig. 3(a)], the amplitude ΔE increases monotonically and saturates slightly as a function of the external field. In contrast, the curves for $T = 0, 0.25$, and 0.5 ps saturate and show an onset of a nonmonotonic behavior clearly indicating that the experiment enters the nonlinear THz regime explained by intraexcitonic Rabi flopping. The phase of the Rabi cycle is set by the pulse area $\theta(T) = \mu_{1s-2p}/\hbar \int_{-\infty}^T |E_{\text{THz}}(t)| dt$, which increases with time T and electric field E_{THz} as seen in Fig. 3.

Beside the amplitude response, electro-optic detection also monitors the phase retardation between external and induced THz fields [Fig. 3(b)]. Since the resonant term ΔE_{THz} and the inductive contribution ΔE_A give rise to different offsets (180° and 90° , respectively), these data provide an elegant way to confirm the presence of both terms. In particular, the experimental phase (blue circles) at $T = -0.25$ ps decreases as a function of $E_{\text{THz}}^{\text{peak}}$ and deviates from 180° to an extent not explicable in a simplified two-level analysis. The theoretical computation with (solid line) and without J_A (dashed line) shows that the intensity dependence of the experimental phase is well explained by the ponderomotive contribution.

In conclusion, we have prepared a dense, dark, and cold $1s$ paraexciton gas in Cu_2O and analyzed its nonlinear THz response in both experiment and theory. Field-sensitive

detection of the reemitted THz transient allows us to monitor the nonlinear many-body dynamics with a sub-cycle temporal resolution. We reveal novel analogies between excitons and atoms including a coherent population transfer from $1s$ to $2p$ orbitals with an efficiency of up to 80% and fingerprints of internal Rabi flopping. At the same time, the phase retardation of the reemitted field points out limitations of the atomlike picture which are well described via a ponderomotive current in our model. The results encourage future implementations of systematic quantum-optical protocols for excitons which may ultimately help to explore their complex phase diagram in hitherto inaccessible regions. The latest advances in high-intensity THz sources will be instrumental in establishing this exciting new research field.

We thank D. Fröhlich for providing the high-quality Cu_2O single crystals and for helpful discussions and H. Stolz and co-workers for making Ref. [21] available to us before publication. This work has been supported by the DFG via the Emmy Noether Program and by the Quantum Optics in Semiconductors Research Group.

- [1] M. H. Anderson *et al.*, *Science* **269**, 198 (1995); K. B. Davis *et al.*, *Phys. Rev. Lett.* **75**, 3969 (1995).
- [2] S. A. Moskalenko and D. W. Snoke, *Bose-Einstein Condensation of Excitons and Biexcitons* (Cambridge University Press, Cambridge, England, 2000).
- [3] D. W. Snoke *et al.*, *Phys. Rev. Lett.* **64**, 2543 (1990); K. E. O'Hara *et al.*, *Phys. Rev. B* **62**, 12909 (2000).
- [4] J. Kasprzak *et al.*, *Nature (London)* **443**, 409 (2006).
- [5] M. Kubouchi *et al.*, *Phys. Rev. Lett.* **94**, 016403 (2005); K. Yoshioka *et al.*, *Phys. Rev. B* **76**, 033204 (2007).
- [6] M. Jörger *et al.*, *Phys. Rev. B* **71**, 235210 (2005).
- [7] J. Brandt *et al.*, *Phys. Rev. Lett.* **99**, 217403 (2007).
- [8] R. Huber *et al.*, *Phys. Rev. Lett.* **96**, 017402 (2006).
- [9] K. Johnsen *et al.*, *Phys. Rev. Lett.* **86**, 858 (2001).
- [10] T. Ideguchi *et al.*, *Phys. Rev. Lett.* **100**, 233001 (2008).
- [11] S. W. Koch *et al.*, *Nature Mater.* **5**, 523 (2006).
- [12] R. Huber *et al.*, *Nature (London)* **414**, 286 (2001).
- [13] R. A. Kaindl *et al.*, *Nature (London)* **423**, 734 (2003); R. Huber *et al.*, *Phys. Rev. B* **72**, 161314(R) (2005).
- [14] I. Galbraith *et al.*, *Phys. Rev. B* **71**, 073302 (2005).
- [15] M. Kira *et al.*, *Prog. Quantum Electron.* **30**, 155 (2006).
- [16] D. Fröhlich *et al.*, *Phys. Rev. Lett.* **55**, 1335 (1985).
- [17] S. G. Carter *et al.*, *Science* **310**, 651 (2005).
- [18] J. R. Danielson *et al.*, *Phys. Rev. Lett.* **99**, 237401 (2007).
- [19] K. Liu *et al.*, *Appl. Phys. Lett.* **85**, 863 (2004); C. Kübler *et al.*, *Appl. Phys. Lett.* **85**, 3360 (2004).
- [20] K. Karpinska *et al.*, *Phys. Rev. B* **72**, 155201 (2005).
- [21] M. French *et al.*, *J. Phys. Condens. Matter* **21**, 015502 (2009).
- [22] J. I. Jang *et al.*, *Phys. Rev. B* **74**, 045211 (2006).
- [23] K. Reimann *et al.*, *Opt. Lett.* **28**, 471 (2003).
- [24] M. Kira *et al.*, *Solid State Commun.* **129**, 733 (2004).
- [25] J. T. Steiner *et al.*, *Phys. Rev. B* **77**, 165308 (2008).